HHS Public Access

Author manuscript

J Photochem Photobiol. Author manuscript; available in PMC 2024 July 12.

Published in final edited form as:

J Photochem Photobiol. 2024 June ; 21: . doi:10.1016/j.jpap.2024.100241.

Photoacoustic lifetime oxygen imaging of radiotherapy-induced tumor reoxygenation *In Vivo*

Jeff Folz[#a,1], **Janggun Jo**[#b,1,2], **Maria E. Gonzalez**[c,d], **Ahmad Eido**[c,d], **Tianqu Zhai**[b], **Roberta Caruso**[c,d], **Celina G. Kleer**[c,d,*], **Xueding Wang**[b,*], **Raoul Kopelman**[a,d,*]

[a]Department of Chemistry, University of Michigan, Ann Arbor, MI 48109, USA

[b]Department of Biomedical Engineering, University of Michigan, Ann Arbor, MI 48109, USA

[c]Department of Pathology, University of Michigan Health System, Ann Arbor, MI 48109, USA

[d]Rogel Cancer Center, University of Michigan Health System, Ann Arbor, MI 48109, USA

[#] These authors contributed equally to this work.

Abstract

Purpose: Early detection and diagnosis of cancer is critical for achieving positive therapeutic outcomes. Biomarkers that can provide clinicians with clues to the outcome of a given therapeutic course are highly desired. Oxygen is a small molecule that is nearly universally present in biological tissues and plays a critical role in the effectiveness of radiotherapies by reacting with DNA radicals and subsequently impairing cellular repair of double strand breaks.

Techniques for measuring oxygen in biological tissues often use blood oxygen saturation to approximate the oxygen partial pressure in surrounding tissues despite the complex, nonlinear, and dynamic relationship between these two separate oxygen populations.

Methods and materials: We combined a directly oxygen-sensitive, tumor-targeted, chemical contrast nanoelement with the photoacoustic lifetime-based (PALT) oxygen imaging technique to

[*]Corresponding authors. kleer@med.umich.edu (C.G. Kleer), xdwang@umich.edu (X. Wang), kopelman@umich.edu (R. Kopelman).
[1]These authors contributed equally to this work.
[2]Statistical Analysis Author.

CRediT authorship contribution statement

Jeff Folz: Writing – review & editing, Writing – original draft, Resources, Project administration, Methodology, Investigation, Formal analysis, Data curation, Conceptualization. **Janggun Jo:** Writing – review & editing, Writing – original draft, Visualization, Validation, Supervision, Software, Resources, Project administration, Methodology, Investigation, Formal analysis, Data curation, Conceptualization. **Maria E. Gonzalez:** Writing – review & editing, Resources, Project administration. **Ahmad Eido:** Methodology, Writing – original draft, Supervision, Resources, Conceptualization. **Tianqu Zhai:** Writing – review & editing, Investigation, Conceptualization. **Roberta Caruso:** Writing – review & editing, Validation, Supervision, Resources, Project administration, Conceptualization. **Celina G. Kleer:** Funding acquisition, Writing – review & editing, Resources, Project administration, Conceptualization, Supervision. **Xueding Wang:** Writing – review & editing, Supervision, Resources, Project administration, Methodology, Funding acquisition, Conceptualization. **Raoul Kopelman:** Writing – review & editing, Supervision, Resources, Project administration.

Declaration of competing interest

The authors declare that they have no known competing financial interests or personal relationships that could have appeared to influence the work reported in this paper.

Supplementary materials

Supplementary material associated with this article can be found, in the online version, at doi:10.1016/j.jpap.2024.100241.

obtain image maps of oxygen in breast cancer tumors in vivo. The oxygen levels of patient-derived xenografts in a mouse model were characterized before and after a course of radiotherapy.

Results: We show that, independent of tumor size, radiotherapy induced an increase in the overall oxygenation levels of the tumor. Further, this increase in the oxygenation of the tumor significantly correlated with a positive response to radiotherapy, as demonstrated by a reduction in tumor volume over the twenty-day monitoring period following therapy and histological staining.

Conclusion: Our PALT imaging presented here is simple, fast, and non-invasive. Facilized by the PALT approach, imaging of tumor reoxygenation may be utilized as a simple, early indicator for evaluating cancer response to radiotherapy. Further characterization of the reoxygenation degree, temporal onset, and possible theragnostic implications are warranted.

Keywords

Cancer; Reoxygenation; Photoacoustics; PACI; Nanosensors; Radiation

Introduction

Cancer is a major health concern worldwide, with almost 2 million new diagnoses and over 600,000 deaths expected in the United States alone in 2023 [1]. Radiation therapy plays a central role in cancer treatment, including breast cancer. The identification of biomarkers able to provide accurate indications of cancer response to radiation therapy are highly desired [2]. Biomarkers take the form of biomolecules, like nucleic acids, proteins, or small molecule metabolites such as folate, phosphocoline, HER-2, and TIMP-1, among many other examples [3–5]. While most of the available biomarkers are specific to certain types of tissues, oxygen is universally present in solid tumors and their surrounding tumor microenvironment (TME).

Oxygen has been identified as a member of the therapy resistance triad [6]. Oxygen's presence is critical for the administration of any radiotherapy, as the incident radiation's generated radicals become fixed in place by bonding with dissolved oxygen [7–9]. Tumors are often hypoxic due to their aberrant metabolism [10]. In addition to radioresistance, hypoxic tumors are often chemoresistant, have genomic instability, show an increased propensity to metastasize, and are associated with a worse patient prognosis [11]. Therefore, measurement of oxygen in the *in-vivo* TME is of great interest when selecting a possible therapeutic avenue.

Notably, the oxygenation within a tumor is dynamic. Hypoxia can be both acute and chronic [12]. Chronic (diffusion limited) hypoxia manifests itself as malformed blood vessels in the TME, i.e., vessels that failed to keep pace with the tumor growth [13,14]. Acute hypoxia arises from the vasculature losing and gaining functionality, or as a result of gas challenge [15–17]. As such, the oxygenation level of a tumor is responsive to perturbations in the TME. Importantly, increases in the local oxygen concentration of the TME have been observed to follow the administration of fractionated radiotherapy [18,19]. The observation of reoxygenation, i.e., increased oxygen content in the TME following radiotherapy, has

been associated with positive treatment outcomes [20,21]. Furthermore, reoxygenation is likely to increase the susceptibility of the remaining cancer cells to radiation therapy [22,23].

Previously, we administered oxygen-sensitive, tumor-targeting and biocompatible chemical contrast nano-elements (TTCENE) to tumor bearing mice [24]. Using photoacoustic lifetime (PALT) oxygen imaging, we, as well as other groups, were able to non-invasively measure the tumor oxygenation levels [24–28]. In a recent study, we showed that tumor oxygenation is correlated with radiotherapeutic efficacy in a mouse model of breast cancer [28]. In the present work, mice bearing patient-derived breast cancers received fractioned radiotherapy, with each mouse receiving 5 Gy of radiation each day, for 5 consecutive days. The tumor oxygenation of each mouse was measured and imaged, using our photoacoustic (PA) and ultrasound (US) dual-modality imaging system, both before the first treatment and after the final radiation fraction was administered on the fifth day. We conclusively demonstrate that our PALT oxygen imaging technique can detect radiotherapy-induced reoxygenation and generate image maps of the TME. Furthermore, we show that the reoxygenation of the TME is correlated with positive therapeutic outcomes. We conclude that this technique has the potential to provide simple, fast, and early diagnostic verification of radiotherapy efficacy and response.

Results

We generated a mouse model of patient-derived breast cancer xenografts (PDX) in NOD/Scid mice. Tumor bearing mice were split into groups based on the size of the tumor and randomly assigned to either a treatment group, which received radiotherapy, or an untreated group that served as a control. As a result, four groups of mice were monitored: radiotherapy treated mice with large (~2 cm^3) tumors, radiotherapy treated mice with small (~1 cm^3) tumors, as well as two control groups, which did not receive radiation, for both large (~2 cm^3) tumors and small (~1 cm^3) tumors. For all groups, tumor oxygenation was assessed via PALT oxygen imaging on the first day, immediately before radiation treatment, and on the last day, following the final dose of radiation treatment. This imaging schedule was selected to evaluate induced changes in tumor oxygenation following the radiotherapeutic course and to relieve mice from the stress of repeated imaging sessions. Control groups did not receive radiation but were imaged on the same schedule. PALT oxygen imaging begins with injecting G2-PAAm nanoparticles into the tail veins of mice. The G2-PAAm nanoparticles are actively targeted to angiogenic vessels via the targeting peptide, F3, and preferentially accumulate in the tumor microenvironment [24]. Previous studies have confirmed the low toxicity and biodistribution profile of the nanoparticles at the administered dose [24,28]. After 1 hour, 630 nm and 920 nm laser excitation are used to excite the oxygen-sensitive G2-PAAm contrast agents and generate oxygen image maps via PALT; oxygen maps are limited to qualitative detection due to unknown deviations in the calibration curve gathered in neat buffer versus the complicated tumor milieu. In both treated groups, each mouse received 5 Gy of radiation every day for 5 consecutive days. This treatment schedule was selected to model a clinically relevant, low-dose fractionated radiotherapy [29]. Changes in tumor volume were monitored for 20 days following the final dose of radiation therapy. Mice were sacrificed and their tumors were histologically evaluated to assess response to radiotherapy (Fig. 1).

The patient-derived xenograft (PDX) tumor model responded positively to the radiation therapy. For both large and small tumors, following radiation treatment, a downward trend in tumor volume can be seen, although large tumors showed a more pronounced absolute change in tumor volume (Fig. 2). In the large tumor group, the average size of tumors decreased from 2312±442 mm^3 on day 0 to 566±153 mm^3 on day 20 after the last treatment; in the small tumor group, the average size of tumors decreased from 1196±245 mm^3 on day 0 to 306 ±148 mm^3 on day 20 after the last treatment. In contrast, in both untreated groups, the tumors continued to grow over the entire monitoring period, with tumor size increased from 2271±260 mm^3 on day 0 to 4091 ±163 mm^3 on day 20 for the large tumor group, and from 1079±108 mm^3 on day 0 to 2923±218 mm^3 on day 20 for the small tumor group.

PALT oxygen images of a tumor, before and after the radiation treatment are shown in Figs. 3a and 3b. The pseudo-color pixels superimposed on the gray-scale US images present the spatially distributed oxygenation level in the tumor. Compared to the image acquired before the treatment as the baseline, the image after treatment shows a clearly increased oxygenation. Figs. 3c and 3d show PALT oxygen images from an untreated tumor as a control. Fig. 3c was acquired when the tumor had a size (1 cm^3) similar to that shown in Fig. 3a. Fig. 3d was acquired 5 days after Fig. 3c but no treatment was performed between these two images. Unlike the treated tumor, results from the untreated tumor indicate that the oxygenation in the TME further decreased after 5 days.

We then assessed the reoxygenation of the TME induced by radiation therapy. With each PALT oxygenation image, a spatial averaging over all the pixels was conducted to give the overall oxygenation level of the TME. Fig. 4 shows the oxygenation level of each individual tumor, before and after radiation therapy, as well as a dotted line showing the trajectory of the change. Fig. 4 also shows the box and whisker plot for each group (i.e., for large and small tumors, with and without radiation therapy). Both large and small tumors showed trajectories of increases in the oxygenation following treatment (Fig. 4a). In large tumors, the TME oxygenation levels increased from 2.20±0.44 % before treatment to 2.85±0.39 % after treatment; in small tumors, the TME oxygenation levels increased from 3.29±1.16 % before treatment to 4.35±1.79 % after treatment. In general, we observe that the changes are larger for small tumors. A similar comparison for untreated tumors is shown in Fig. 4b. In the control groups (untreated tumors), the “after’ measurements were performed 5 days following the baseline measurements (before), and no radiation therapy was performed between them. We found that tumors that were not exposed to radiation treatment had an overall decrease in their oxygenation during the monitoring period, indicating that without therapeutic intervention the tumors became more hypoxic after 5 days. For large tumors, the TME oxygenation levels decreased from 2.03±0.90 % to 1.01±0.76 %; for small tumors, the TME oxygenation levels decreased from 2.53±0.83 % to 2.10±0.71 %. Interestingly, here the magnitude of the change was greater for the large tumors than it was for the small tumors – the opposite of the treated case. The latter may be expected due to easier oxygen diffusion from nearby normal tissue, or an increased Warburg effect [10].

We further evaluated whether PALT oxygen imaging can differentiate between the treated and the untreated tumors, in both small and large size tumor groups. In Fig. 5a, the average changes in TME oxygenation levels, for each tumor group after radiation therapy, are

presented. For large tumors, with and without being treated by radiation therapy, the changes of oxygen levels are 0.65±0.57 % and −1.02±1.25 %, respectively. For small tumors, with and without being treated by radiation therapy, the changes of oxygen levels are 1.06±0.75 % and −0.43±0.51 %, respectively. Consistent with our findings described above, unlike the treated tumor groups which showed improvement in TME oxygenation levels after radiation therapy, the untreated tumor groups showed negative changes in oxygenation levels, indicating that the tumors without treatment became more hypoxic. We next created a scatterplot of the change in tumor size, relative to the change in tumor oxygenation, that clearly illustrates how the four tumor groups formed distinct clusters (Fig. 5b). Both treated tumor groups clustered into the same region of the plot, which corresponds to an increase in oxygenation following radiotherapy, and a subsequent decrease in tumor volume following the monitoring period. In contrast, the untreated tumor groups kept growing during the monitoring period, and tended to have small, negative changes in tumor oxygenation.

To compare the radiation therapy effects in the treated and untreated tumor groups, the hematoxylin and eosin (H&E)-stained tumors were analyzed, as shown in Fig. 6. In contrast to the untreated tumors, the PDX tumors treated with radiation show large areas of treatment effect, characterized by stromal hyalinization with reduced cancer cell cellularity, resembling what is observed in clinical pathology practice. Additional histological images gathered from other tumors may be found in the supplementary information.

Discussion

Oxygen-sensing nanoparticles were administered to mice bearing breast cancer PDX tumors. Using PALT oxygen imaging, the oxygenation of the TME was characterized in vivo. Mice were divided by tumor size and split into treatment and control (no treatment) groups. Radiation therapy was given to the treatment groups every day for five consecutive days. Tumor oxygenation was again measured using PALT oxygen imaging, and the tumor volume was monitored for an additional 20 days. We observed that mice, bearing either small (~1 cm^3) or large (~2 cm^3) tumors, when treated by radiotherapy, showed a decrease in tumor volume over the monitoring period, as expected. Furthermore, both treatment groups showed an increase in their average tumor oxygenation levels following radiotherapy. In contrast, the untreated control groups showed the opposite trends: their tumor volumes continued to increase over the monitoring period, and they showed a decrease in tumor oxygenation between the two measurements separated by five days. It is noteworthy that the oxygenation of the larger tumors improved less than that of the smaller tumors. We attribute the poor reoxygenation to increased proportions of necrotic tissue in the larger tumor groups.

Increases in oxygenation of the TME following radiotherapy have been previously observed [20–33]. It was suggested that tumor reoxygenation may be caused by a reduction in the oxygen consumption rate of the tumoral cells [34]. As such, there is evidence that the oxygen response to radiation can be used to differentiate between radio-sensitive and radio-resistant tumors [35]. This study observed reoxygenation around an hour after the final radiotherapy dose with percent oxygen level changes around ~1 %; similar changes have been reported using the OxyLab pO_2 system 24 h post radiation [36]. Other studies have observed the effect as soon as 30 min [32].The temporal manifestation of reoxygenation

needs further characterization, as does the dependence of the reoxygenation phenomenon on the radiation administration rate and dose.

Several techniques exist to probe and characterize the reoxygenation events. A review comparing various photoacoustic approaches and alternative oxygen-sensing methods has been published recently [37]. Porphyrin molecules, and their many derivatives, have long been employed for oxygen measurements based on phosphorescence quenching [38,39]. Porphyrins have been applied to oxygen visualization [40], *in vivo* measurements of bone marrow oxygen [41], and measurement of oxygen depletion following FLASH radiation [42,43]. A notable advantage of using porphyrin contrast agents is the ability to monitor tissue oxygenation (pO_2) directly, rather than having to rely on blood oxygenation (sO_2) level as a proxy. This approach allows researchers to directly probe the oxygen molecules that would be available for enhancing the effects of radiotherapy. We further argue that our nanoparticle-enhanced PALT approach has several addition advantages: i) encapsulation of the porphyrin in an inert matrix protects the porphyrin from the environment and minimizes deviations in the calibration between neat buffer and the messy TME, enabling measurements of oxygenation, ii) encapsulation enhances solubility and enables active targeting of the porphyrin molecule to the TME, and iii) a photoacoustic approach allows for better spatial resolution in the final image. In comparison, direct measurement of phosphorescence quenching boasts an easier experimental approach and outstanding temporal resolution.

One disadvantage of exogenous contrast agents is the added concern regarding the biodistribution of the agent in regards to the biodistribution of oxygen, which cannot be assumed to be similar. Techniques like Oxygen-enhanced Magnetic Resonance Imaging (MRI) have already been used preclinically to monitor changes in tumor oxygenation induced by radiotherapies [31,32]. However, MRI machines are expensive, limited to patients without metallic implants, and suffer from relatively poor temporal resolution. Similarly, approaches using the even more expensive method of positron emission tomography (PET) with fluorine-18 (F-18) also involve expensive chemical contrast agents that must be prepared on site [33]. Notably, both PET and PALT oxygen imaging rely on exogenous contrast agents, while MRI and DRS measure analytes in their native environment. In the latter case, as with pulse oximetry, oxygen-bound to hemoglobin (sO_2) is being used as a proxy for dissolved tissue oxygen (pO_2). However, the relationship between these two measures is nonlinear [44] and the latter is likely more relevant in the context of radiation therapy. Each oxygen measurement approach has advantages and disadvantages relative to the others. Researchers can tailor their approach based on their experimental needs and the nature of the question being interrogated. Based on our data, our nanoparticle-enhanced PALT imaging method is a fast, easy, and relatively inexpensive approach for probing tumor reoxygenation following therapeutic intervention, with potential clinical applications.

Finally, it should be noted that while many excellent examples of theranostic approaches combining imaging and therapy exist in the literature [45–47], the therapeutic capabilities of the G2-PAAm remain uncharacterized. Embedded in a relatively inert polyacrylamide matrix, it seems unlikely that the G2-PAAm nanoparticles would display any significant

radiosensitizing capability, but this variable was never explicitly interrogated. Similarly, the mechanism of phosphorescent quenching necessarily results in the production of singlet oxygen, which may in turn result in phototoxicity at the tumor site. We note that both treated and untreated tumors were imaged in the same manner with the same nanoparticle dose, but extent and efficacy of any photodynamic effect imparted by the nanoparticles was uncharacterized. We argue that this effect can only be beneficial, if superficially.

Methods

Nanoparticle synthesis

Targeted G2 oxyphor polyacrylamide nanoparticles were synthesized via previously reported methods [24]. The biocompatibility of the same nanoparticles was demonstrated previously [24,28]. Unless otherwise indicated, all chemicals were purchased from MilliporeSigma. Briefly, a monomer solution containing G2 oxyphor (4.0 mg, 1.3 μmol, Oxygen Enterprises, Ltd.), 3-(aminopropyl) methacrylamide hydrochloride salt (53.6 mg, 0.300 mmol), acrylamide (690 mg, 9.7 mmol), 1-ethyl-3-(3-(dimethylamino)propyl) carbodiimide (2.9 mg, 15 μmol, ThermoFisher Scientific), and sulfo-N-hydroxysuccinimide (8.2 mg, 37 μmol, ThermoFisher Scientific) dissolved in phosphate-buffered saline (pH 7.4, 1.3 mL) (PBS) was prepared and stirred for 2 h under dark conditions. Then 3-(acryloylxy) −2-hydroxypropyl methacrylate (321 mg, 1.50 mmol) was added, completing the monomer solution.

Separately, an oil phase was prepared in a 100 mL round-bottom flask containing hexane (45 mL), dioctyl sulfosuccinate sodium salt (1.6 g, 3.6 mmol), and Brij L4 (3.3 mL, 8.6 mmol). This oil phase was purged using argon gas and kept under the inert atmosphere with vigorous stirring. After a minimum of 20 min of purging with the inert gas, the previously prepared monomer solution was injected into the oil phase, which was then further purged for a minimum of 20 min. Polymerization was initiated by first injecting 100 μL N,N,N’,N’-tetramethylethylenediamine (0.67 mmol) into the round-bottom flask, followed by 100 μL of a 10 % (w/v) ammonium persulfate (44 μmol) solution in PBS. The reaction mixture was then stirred for 2 h under the inert atmosphere. The reaction was quenched by exposing it to air for 5 min before the hexane was removed by rotary evaporation. The prepared nanoparticles were washed with ethanol and water, with an Amicon Filter Cell using a 300 kDa filter. The obtained nanoparticles (G2-PAAm) were then lyophilized.

To actively target G2-PAAm nanoparticles to the tumor area, the nanoparticles’ surface was conjugated with F3 peptides. A PBS solution (pH 7.4, 2.5 mL) containing G2-PAAm nanoparticle (50 mg) and bifunctional polyethylene glycol (4 mg, MAL-PEG-SCM, 2 kDa, Creative PEGWorks) was stirred for 30 min. The mixture was then washed 3 times with PBS, using an Amicon Ultra Centrifugal Filter (100 kDa) to remove the unreacted PEG. After the washes, the solution was resuspended to its original concentration (50 mg/2.5 mL) and the F3 peptide (11 mg, 3.2 μmol, KDEPQRRSARLSAKPAPPKPEPKPKKAPAKKC, RS Synthesis) was added. The solution was stirred overnight. Then, on the next day, cysteine (0.63 mg, 5.2 μmol) was added to quench the unreacted maleimide groups and stirred for 2 h. The solution was then washed again to remove the unreacted F3 and cysteine, and then lyophilized.

Animal models

Orthotopic PDX mouse models of breast cancer were used in this study. The tumor samples (J000100675, Jackson Laboratory, ME), derived from a breast cancer patient (female, 56 year-old, white, AJCC IIB, grade 3 and treatment naive) were implanted in the abdominal mammary fat pads of immunodeficient mice (NOD.Cg-Prkdcscid Il2rgtm-1Wjl/SzJ or NSG) to created PDX tumors which recapitulate the genetic and biochemical attributes of the original patient's tumor [48]. When the sizes of the PDX tumors reached the desired volumes (1–2 cm^3), the mice were used for the PALT oxygen imaging experiment and the radiation therapy.

Experimental procedure of tumor imaging

All animal experiments followed the protocol approved by the Institutional Animal Care and Use Committee (IACUC) at the University of Michigan (Protocol: PRO00009561). The mice were anesthetized with isoflurane during the imaging and therapy processes. Before imaging, oxygen sensing G2 Polyacrylamide nanoparticles (G2-PAAm NPs), conjugated with tumor-targeting F3 peptides, were administrated systematically through the tail vein (20 mg/mL in PBS, 0.1 mL). The PALT oxygen imaging was conducted around 1 hour after the injection, with the contrast of the tumor enhanced by the PAAm NPs. The setup for PALT oxygen imaging was similar to that reported in our previous studies [24,28]. For each tumor, 2D B-scan imaging was conducted through the center of the tumor. While the temperature of mice was not actively controlled or measured during imaging, all mice were exposed to less than 2 min of laser radiation for PALT imaging. Photoacoustic-induced heating is known to be minimal, and increases in temperature return to baseline within microseconds [49]. Two lasers, for the pump beam at 630 nm (Surelite OPO, Amplitude, CA) and the probe beam at 920 nm (Phocus Mobile, OPOTEK, CA), covered the imaging region of the PDX tumor. At the 630 nm wavelength, the light fluence on the mouse's skin was approximately 10 mJ/cm^2. This applied light fluence was well below the 20 mJ/cm^2 safety limit set by the American National Standard Institute (ANSI) at the selected wavelength. The light should have minimal effect on the biological tissue during imaging, but will be sufficient to pump the contrast agent to the excited state. PA signals were collected using a PA-US dual-modality imaging system built on a Verasonics research ultrasound unit (Vantage, Verasonics, WA) with a linear array probe working at a central frequency of 18 MHz (L22–14v, Verasonics, WA). The lateral and axial resolutions of the PA imaging, using this system, were 205 μm and 218 μm, respectively, at a 10 mm depth. With varying delays of 10, 20, 30, 40 and 50 μs between the pump beam and the probe beam, the PALT oxygen image of each tumor was produced by following the same process as previously reported [24]. We used a needle type oximeter (Microx TX3 Presens, Regensburg, Germany) to set up the PALT calibration, as described in our previous study [24]. At different oxygen concentrations, the linear correlations between decay rates and oxygen concentrations were measured. During tumor imaging, the system acquired 2D B-scan PA and US images simultaneously when the animal was under anesthesia using isoflurane mixing with over 99 % oxygen gas. For each result, the PALT oxygen image was presented in pseudo-color and superimposed on the gray-scale US image, to show both the spatially distributed functional information and the tissue structures.

Experimental procedure of tumor treatment

After an initial round of PALT oxygen imaging, each mouse was treated with radiation therapy daily for 5 consecutive days. Mice were anesthetized with isoflurane and over 99 % oxygen gas prior to treatment. Irradiations were performed using a Kimtron IC 225 (Kimtron Medical), at a dose of approximately 5 Gy, at the University of Michigan Comprehensive Cancer Center Experimental Irradiation Core (Ann Arbor, MI). X-rays generated were on the order of 200–250 keV. Dosimetry was performed semiannually using an ionization chamber connected to an electrometer system that was directly traceable to a National Institute of Standards and Technology calibration. The beam was collimated, and a 2-mm Cu beam hardening filter was utilized. On the fifth day, following irradiation, the mice were once again imaged using the above-described procedure. Following the last dose of radiation and after the last PALT oxygen imaging, the tumor size of each mouse was monitored over a total period of 20 days to determine the change in tumor volume. Both treated and untreated tumors were harvested, cut, and stained with H&E for histological examination.

Statistical analysis

In the analysis of statistical significance, two-sample *t*-tests were conducted using the built-in functions of MATLAB® (R2022b, Mathworks, Natick, Massachusetts).

Supplementary Material

Refer to Web version on PubMed Central for supplementary material.

Acknowledgement

The authors would like to thank Dr. Sergei A. Vinogradov for his generous donation of G2 oxyphor.

Funding Statement

This work was supported by National institutes of Health (NIH) grants R01CA125577 and R01CA107469 (C.G.K.), NIH/NCI grants R01CA250499 (to XW, RK, CK), Prostate Cancer Foundation grant 19YOUN12 (JJ), Department of Defense Breast Cancer Research Program grant W81XWH-19–1-0093 (C.G.K) and University of Michigan Rogel Cancer Center support grant P30CA046592. C.G.K. is a Rogel Scholar.

Data availability

Data will be made available on request.

Data availability statement

Research data are stored in an institutional repository and will be shared upon request to the corresponding author.

References

[1]. Siegel RL, Miller KD, Wagle NS, Jemal A, Cancer statistics, 2023, CA: Cancer J. Clin. 73 (Jan 12, 2023) 17–48. [PubMed: 36633525]

[2]. Sarhadi VK, Armengol G, Molecular biomarkers in cancer, Biomolecules 12 (Jul 23, 2022) 1021. [PubMed: 35892331]

[3]. Hu J, Juan W, Sahyoun NR, Intake and biomarkers of folate and risk of cancer morbidity in older adults, NHANES 1999–2002 with medicare linkage, PLoS ONE 11 (2) (Feb 10, 2016) e0148697.

[4]. Rakha EA, El-Sayed ME, Green AR, Lee AHS, Roberrtson JF, Ellis IO, Prognostic markers in triple-negative breast cancer, Cancer 109 (1) (Jan 1, 2007) 25–32. [PubMed: 17146782]

[5]. Szász AM, Lanczky A, Nagy A, et al. , Cross-validation of survival associated biomarkers in gastric cancer using transcriptomic data of 1,065 patients, Oncotarget 7 (31) (Aug 2, 2016) 49322–49333. [PubMed: 27384994]

[6]. Lee CH, Folz J, Tan JWY, Jo J, Wang X, R Kopelman, Chemical imaging in vivo: photoacoustic-based 4-dimensional chemical analysis, Anal. Chem. 91 (4) (Jan 14, 2019) 2561–2569. [PubMed: 30638359]

[7]. Rockwell S, Dobrucki IT, Kim EY, Marrison ST, Vu VT, Hypoxia and radiation therapy: past history, ongoing research, and future promise, Curr. Mol. Med. 9 (4) (May 2009) 442–458. [PubMed: 19519402]

[8]. Harrison LB, Chadha M, Hill RJ, Hu K, Shasha D, Impact of tumor hypoxia and anemia on radiation therapy outcomes, Oncologist 7 (6) (2002) 492–508. [PubMed: 12490737]

[9]. Tredan O, Galmarini CM, Patel K, Tannock IF, Drug resistance and the solid tumor microenvironment, J. Natl. Cancer Inst. 99 (19) (Oct 3, 2007) 1441–1454. [PubMed: 17895480]

[10]. Warburg O, Wind F, Negelein E, The metabolism of tumors in the body, J. Gen. Physio. 8 (6) (Mar 7, 1927) 519–530.

[11]. Vaupel P, Mayer A, Hypoxia in cancer: significance and impact on clinical outcome, Cancer Metastasis Rev 26 (2) (Jun 2007) 225–239. [PubMed: 17440684]

[12]. D'Alonzo RA, Gill S, Rowshanfarzad P, et al. , In vivo noninvasive preclinical tumor hypoxia imaging methods: a Review, Int. J. Radiat Biol. 97 (5) (Apr 7, 2021) 593–631. [PubMed: 33703994]

[13]. Gallez B, Baudelet C, Jordan BF, Assessment of tumor oxygenation by electron paramagnetic resonance: principles and applications, NMR Biomed 17 (5) (Aug 2004) 240–262. [PubMed: 15366026]

[14]. Watabe T, Kanai Y, Ikeda H, et al. , Quantitative evaluation of oxygen metabolism in the intratumoral hypoxia: 18F-fluoromisonidazole and 15O-labelled gases inhalation PET, EJNMMI Res 7 (Feb 16, 2017) 16. [PubMed: 28210996]

[15]. Ebbesen P, Pettersen EO, Gorr TA, et al. , Taking advantage of tumor cell adaptations to hypoxia for developing new tumor markers and treatment strategies, J Enzyme Inhib. Med. Chem 24 (2009) 1–39.

[16]. Fleming IN, Manavaki R, Blower PJ, et al. , Imaging tumour hypoxia with positron emission tomography, Br. J. Cancer 112 (Dec 16, 2014) 238–250. [PubMed: 25514380]

[17]. Hall EJ, Giaccia AJ, Radiobiology For The Radiologist, Lippincott Williams & Wilkins, Philadelpha, PA, 1972.

[18]. Brown JM, Tumor hypoxia in cancer therapy, Methods Enzymol 435 (2007) 295–321.

[19]. Potiron VA, Abderrahmani R, Clement-Colmou K, et al. , Improved functionality of the vasculature during conventionally fractionated radiation therapy of prostate cancer, PLoS ONE 8 (12) (Dec 31, 2013) e84076.

[20]. Ressel A, Weiss C, Feyerabend T, Tumor oxygenation after radiotherapy, chemotherapy, and/or hyperthermia predicts tumor free survival, Int. J. Radiat. Oncol. Biol. Phys 49 (4) (Mar 15, 2001) 1119–1125. [PubMed: 11240254]

[21]. Milas L, Hunter NR, Mason KA, et al. , Role of reoxygenation in induction of enhancement of tumor radioresponse by paclitaxel, Cancer Res 55 (15) (Aug 15, 1995) 3564–3568. [PubMed: 7627965]

[22]. Crokart N, Jordan BF, Baudelet C, et al. , Early reoxygenation in tumors after irradiation: determining factors and consequences for radiotherapy regimens using daily multiple fractions, Int. J. Radiat. Oncol. Biol. Phys. 63 (3) (Nov 1, 2005) 901–910. [PubMed: 16199320]

[23]. Chen Z, Guo W, Wu Q, et al. , Tumor reoxygenation for enhanced combination of radiation therapy andmicrowave thermal therapy using oxygen generation in situ by CuO

nanosuperparticles under microwave irradiation, Theranostics 10 (10) (Mar 25, 2020) 4659–4675. [PubMed: 32292521]

[24]. Jo J, Lee CH, Folz J, et al. , In vivo photoacoustic lifetime based oxygen imaging with tumor targeted G2 polyacrylamide nanosonophores, ACS Nano 13 (12) (Dec 24, 2019) 14024–14032. [PubMed: 31820930]

[25]. Ray A, Rajian JR, Lee YE, Wang X, Kopelman R, Lifetime-based photoacoustic oxygen sensing in vivo, J. Biomed. Opt. 17 (5) (May 17, 2012) 057004.

[26]. Punnoose J, Nachman H, Ashkenazi S, Oxygen imaging for non-invasive metastasis detection, Sensors (Basel) 22 (1) (Dec 29, 2021) 237. [PubMed: 35009780]

[27]. Shao Q, Morgounova E, Jiang C, et al. , In vivo photoacoustic lifetime imaging of tumor hypoxia in small animals, J. Biomed. Opt. 18 (7) (Jul 22, 2013) 076019.

[28]. Jo J, Folz J, Gonzalez ME, et al. , Personalized oncology by in vivo chemical imaging: photoacoustic mapping of tumor oxygen predicts radiotherapy efficacy, ACS Nano 17 (5) (Feb 27, 2023) 4396–4403. [PubMed: 36847392]

[29]. Laine AM, Pompos A, Timmerman R, et al. , The Role of Hypofractionated Radiation Therapy with Photons, Protons, and Heavy Ions for Treating Extracranial Lesions, Front. Oncol. 5 (Jan 2016) 302. [PubMed: 26793619]

[30]. Jules A, Means D, Troncoso JR, et al. , Diffuse reflectance spectroscopy of changes in tumor microenvironment in response to different doses of radiation, Radiat. Res. 198 (6) (Dec 1, 2022) 545–552. [PubMed: 36240754]

[31]. Salem A, Little RA, Latifn A, et al. , Oxygen-enhanced MRI is feasible, repeatable, and detects radiotherapy-induced change in hypoxia in xenograft models and in patients with non-small cell lung cancer, Clin. Cancer Res. 25 (13) (Jul 1, 2019) 3818–3829. [PubMed: 31053599]

[32]. Qian J, Yu X, Li B, et al. , In vivo monitoring of oxygen levels in human brain tumor between fractionated radiotherapy using oxygen-enhanced MR imaging, Curr. Med. Imaging. 16 (4) (2020) 427–432. [PubMed: 32410542]

[33]. Narita T, Aoyama H, Hirata K, et al. , Reoxygenation of glioblastoma multiforme treated with fractionated radiotherapy concomitant with temozolomide: changes defined by 18F-fluoromisonidazole positron emission tomography: two case reports, Jpn. J. Clin. Oncol. 42 (2) (Feb 2012) 120–123. [PubMed: 22198964]

[34]. Dadgar S, Troncoso JR, Sigel ER, et al. , Spectroscopic investigation of radiation-induced reoxygenation in radiation-resistant tumors, Neoplasia 23 (1) (Jan 2021) 49–57. [PubMed: 33220616]

[35]. Diaz PM, Jenkins SV, Alhallak K, et al. , Quantitative diffuse reflectance spectroscopy of short-term changes in tumor oxygenation after radiation in a matched model of radiation resistance, Biomed. Opt. Express. 9 (8) (Aug 1, 2018) 3794–3804. [PubMed: 30338156]

[36]. Harriss W, Bezak E, Yeoh E, Hermans M, Measurement of reoxygenation during fractionated radiotherapy in head and neck squamous cell carcinoma xenografts, Australas. Phys. Eng. Sci. Med. 33 (3) (Sep 2010) 251–263. [PubMed: 20878297]

[37]. Nasri D, Manwar R, Kaushik A, Er EE, Avanaki K, Photoacoustic imaging for investigating tumor hypoxia: a strategic assessment, Theranostics 13 (10) (May 2023).

[38]. Vinogradov SA, Wilson DF, Extended porphyrins. New IR phosphors for oxygen measurements, Adv Exp Med Biol 411 (1997) 597–603. [PubMed: 9269478]

[39]. Dunphy I, Vinogradov SA, Wilson DF, Oxyphor R2 and G2: phosphors for measuring oxygen by oxygen-dependent quenching of phosphoirescence, Anal. Biochem. 310 (2002) 191–198. [PubMed: 12423638]

[40]. Roussakis E, Li Z, Nowell NH, Nichols AJ, Evans CL, Bright, “clickable” porphyrins for the visualization of oxygenation under ambient light, Angew. Chem. Int. Ed. 54 (2015) 14728–14731.

[41]. Spencer J, Ferraro F, Roussakis E, et al. , Direct measurement of local oxygen concentration in the bone marrow of live animals, Nature 508 (2014) 269–273. [PubMed: 24590072]

[42]. Van Slyke AL, El Khatib M, Velalopoulou A, Diffenderfer E, Shoniyozov K, Kim MM, Karagounis IV, Busch TM, Vinogradov SA, Koch CJ, D Wiersma R, Oxygen Monitoring in

Model Solutions and In Vivo in mice during proton irradiation at conventional and FLASH dose rates, Radiat Res 198 (2) (2022 Aug 1) 181–189. [PubMed: 35640166]

[43]. El Khatib M, Motlagh AO, Beyer JN, Troxler T, Allu SR, Sun Q, Burslem GM, A Vinogradov S, Direct measurements of FLASH-induced changes in intracellular oxygenation, Int J Radiat Oncol Biol Phys 118 (3) (2024 Mar 1) 781–789. [PubMed: 37729972]

[44]. Madan A, Correlation between the levels of $SpO_2$and PaO_2, Lung India 34 (3) (2017) 307–308. May-Jun. [PubMed: 28474668]

[45]. Li H, Wu Z, Zhang J, Sun X, Duan F, Yao J, Sun M, Zhang J, Nie L, Instant ultrasound-evoked precise nanobubble explosion and deep photodynamic therapy for tumors guided by molecular imaging, ACS Appl Mater Interfaces 13 (18) (2021 May 12) 21097–21107. [PubMed: 33908256]

[46]. Chen R, Huang S, Lin T, Ma H, Shan W, Duan F, Lv J, Zhang J, Ren L, Nie L, Photoacoustic molecular imaging-escorted adipose photodynamic-browning synergy for fighting obesity with virus-like complexes, Nat Nanotechnol 16 (4) (2021 Apr) 455–465. [PubMed: 33526836]

[47]. Peng Y, Liu Y, Lu X, Wang S, Chen M, Huang W, Wu Z, Lu G, Nie L, Ag-Hybridized plasmonic Au-triangular nanoplates: highly sensitive photoacoustic/Raman evaluation and improved antibacterial/photothermal combination therapy, J. Mater. Chem. B. 6 (2018) 2813–2820. [PubMed: 32254234]

[48]. Tentler JJ, Tan AC, Weekes CD, et al. , Patient-derived tumour xenografts as models for oncology drug development, Nat. Rev. Clin. Oncol. 9 (6) (Apr 17, 2012) 338–350. [PubMed: 22508028]

[49]. Wang LV, Multiscale photoacoustic microscopy and computed tomography, Nat. Photonics. 3 (Aug 28, 2009) 503–509. [PubMed: 20161535]

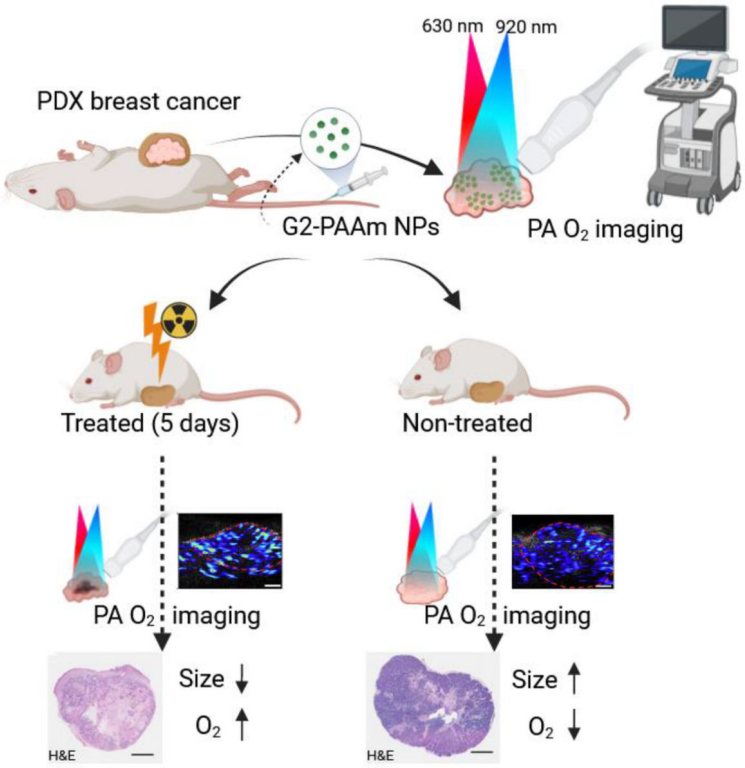

Fig. 1.

A schematic summary of the experimental approach. Oxygen-sensitive nanoparticles (G2-PAAm) are injected into the tail veins of mice bearing PDX tumors. Upon arrival in the tumor microenvironment, G2-PAAm are excited by 630 nm (pump) and 920 nm (probe) laser light so that photoacoustic oxygen image maps may be generated. Treated mice were then given a course of radiotherapy before being imaged again, with the untreated group receving no therapy and serving as a control. Following radiotherapy and imaging, mice were sacrificied and their tumors histologically evaluated. Arrows indicate whether the measure increased or decreased during the monitoring period.

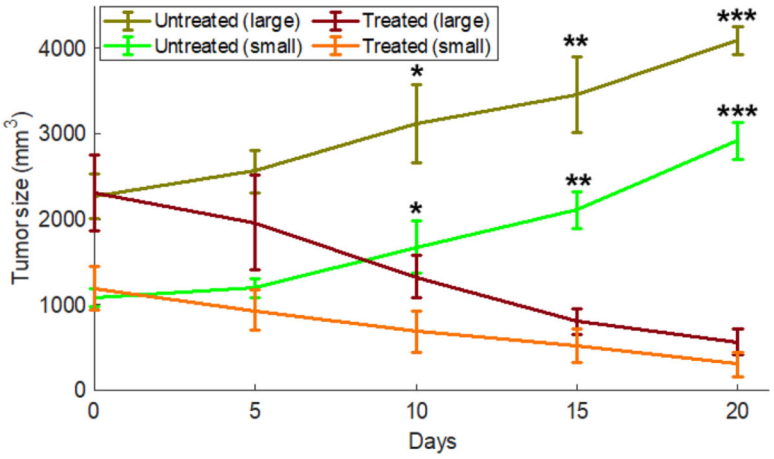

Fig. 2.

The change in tumor volume for each treatment group over a period of 20 days after radiation treatment. The results from four groups of animals are presented, including large tumors treated by radiation therapy ($n = 6$), small tumors treated by radiation therapy ($n = 6$), large tumors without being treated by radiation therapy ($n = 5$), and small tumors without being treatment by radiation therapy ($n = 4$). The measurement on each time point shows the mean ± standard deviation. * indicates that $p < 0.001$ in a two-sample t-test when comparing to the baseline measurement at day 0, while ** indicates $p < 1.0e^{-5}$, and *** $p < 1.0e^{-7}$.

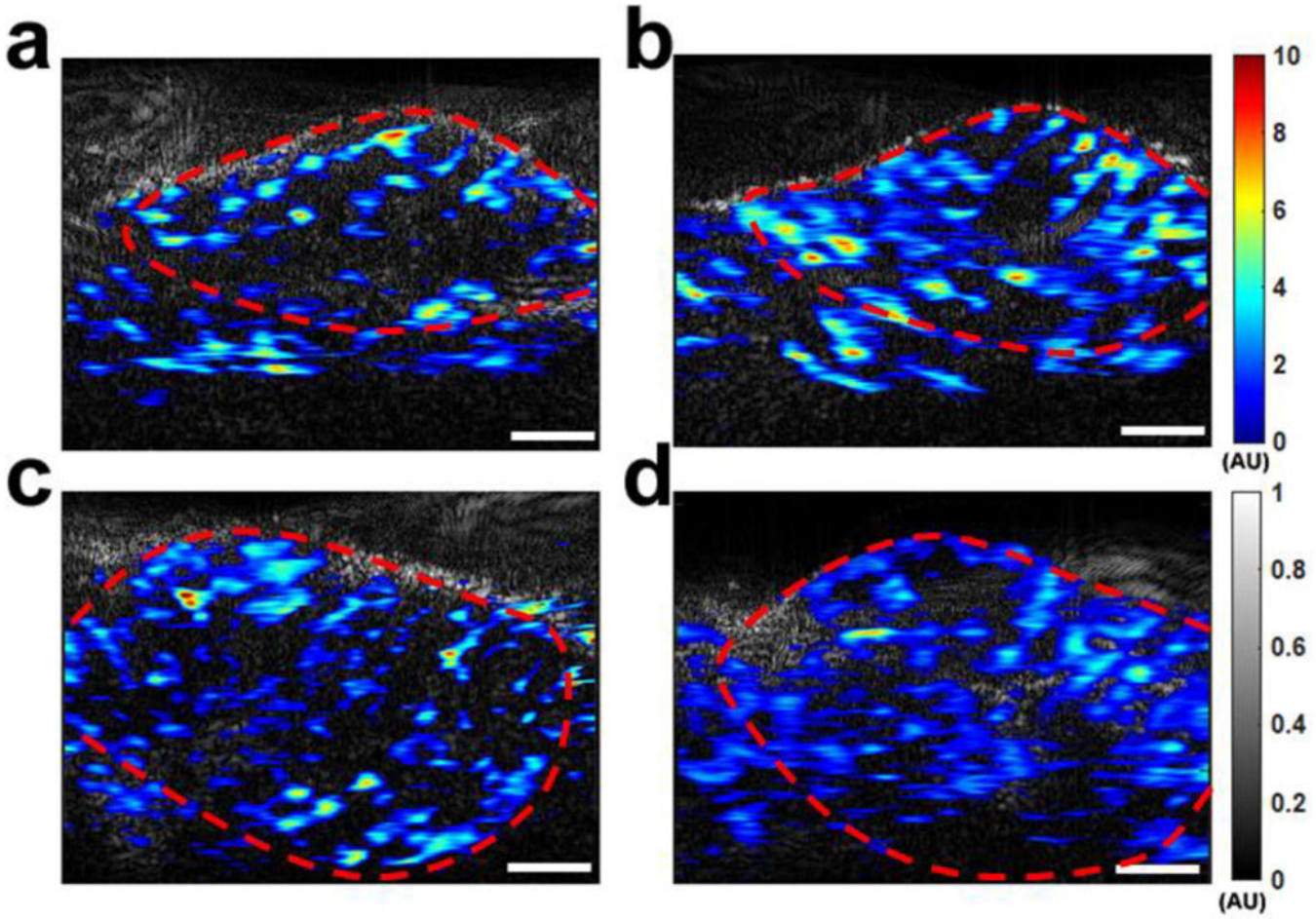

Fig. 3.

PALT oxygen images of tumors in vivo. (a) Representative oxygen map of the tumor before treatment using radiation therapy. (b) Representative oxygen map of the same tumor of (a) after 5 days of treatment. (c) Representative oxygen map of an untreated tumor. (d) Representative oxygen map of the same tumor of (c) after 5 days without treatment. In each image, the tumor area is marked by a dashed line. Each PALT oxygen image in pseudo-color is superimposed on the US image showing the tissue structure. The scale bar is 2 mm.

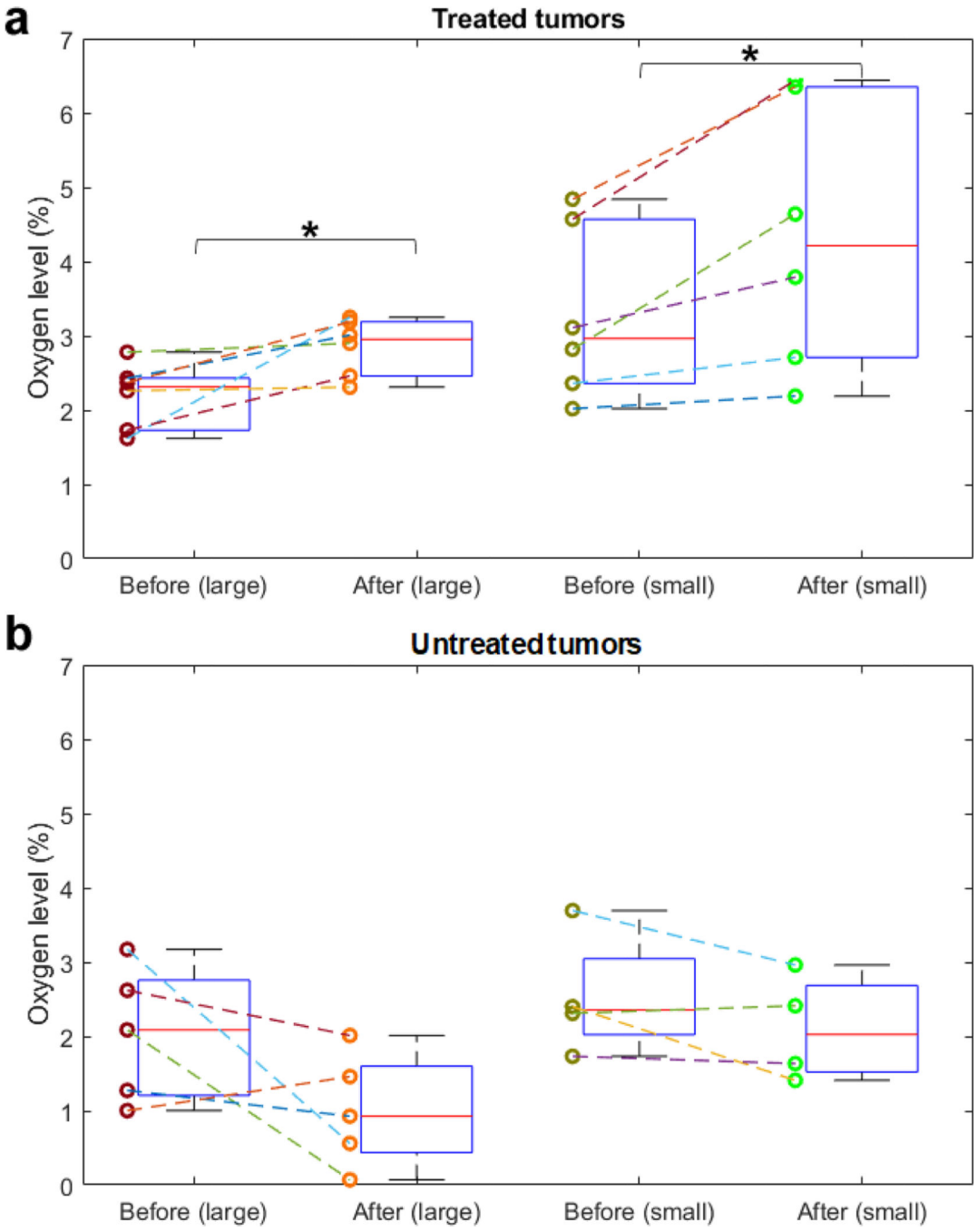

Fig. 4.

Trajectories of individual tumor's change in oxygenation level in responding to radiation therapy, as well as the box and whisker plot for each tumor group. Boxes show the median and interquartile range. (a) TME oxygenation levels for the treated tumor groups before and after radiation therapy. Both small and large tumors displayed an increase in oxygenation following radiotherapy. The p values showing statistically significant differences are 0.038 for large tumors and 0.0183 for small tumors. (b) TME oxygenation levels for the untreated tumor groups. Here, for both large and small untreated tumors, the oxygenation of the TME

decreased over the monitoring period. Changes in untreated tumors were not statistically significant. * indicates $p < 0.05$.

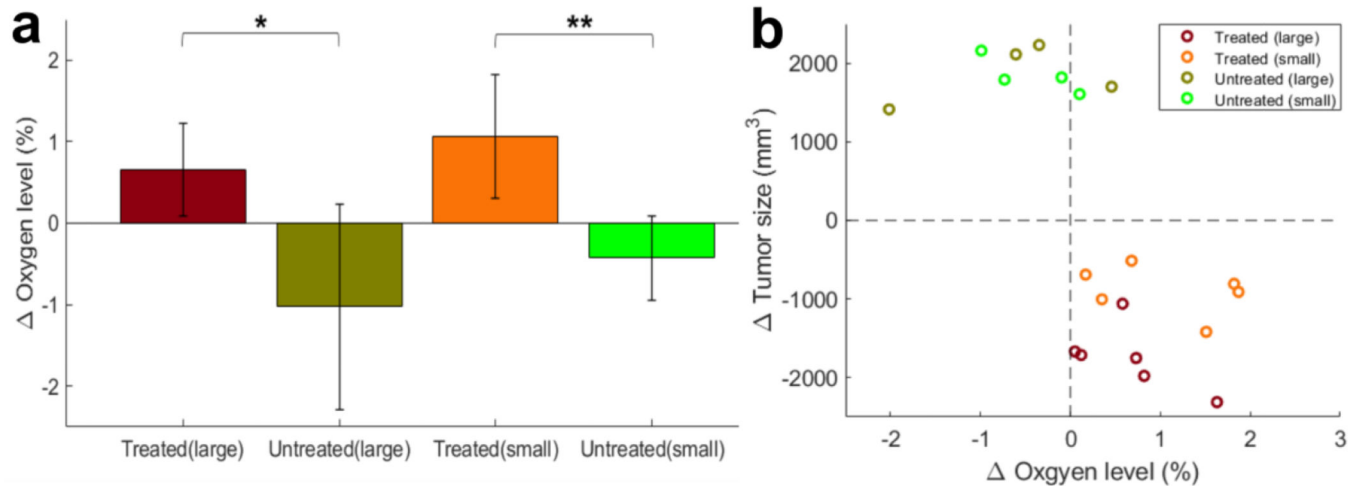

Fig. 5.

Changes in tumor oxygen level for each subset of tumor sizes and treatment. (a) A column graph showing the average changes in the TME's oxygenation levels for the four tumor groups. Both large and small size tumors that received radiation therapy showed increases in their TME oxygenation levels; while both large and small size tumors in the control groups without treatment showed decreases in their TME oxygenation levels. Error bars represent the standard deviation of the means. * indicates $p < 0.05$ and ** indicates $p < 0.01$ in two-sample *t*-tests; the calculated p values were 0.016 ($p < 0.05$) for large size tumors and 0.009 ($p < 0.01$) for small size tumors, when comparing the treated and untreated tumor groups. (b) A scatter plot showing how each of the treatment groups cluster based on their treatment responses. Change in tumor size was monitored over 20 days, while change in oxygen level refers to before and after 5 days of radiation therapy. Both treated tumor groups had positive changes in TME oxygenation and negative changes in tumor volume. The opposite trend was observed for the untreated tumor groups: positive changes in tumor volume accompanied by negative changes in TME oxygenation.

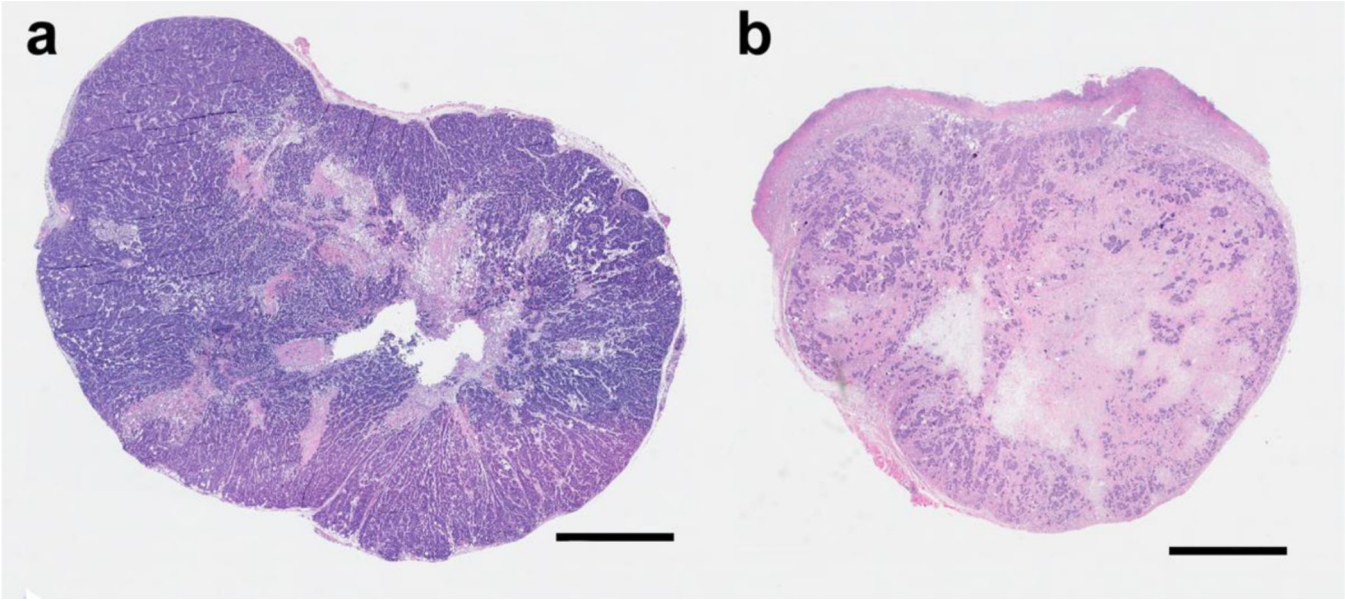

Fig. 6.

Representative images of whole mounts of PDX tumors stained with H&E. (a) Histology slide from an untreated tumor monitored for 20 days without radiation therapy. (b) Histology slide from a treated tumor that received 5 Gy of radiation each day for 5 consecutive days and was monitored for 20 days. Note the areas of hyalinization and necrosis with scant tumor nests due to the radiation therapy. The scale bar is 2 mm.